Oxidation Resistance of Magnetron Sputter Deposited β-FeAl+Zr Coatings

Zhenyu Liu[1], Wei Gao[1], and Fuhui Wang[2]

[1]*Department of Chemical and Materials Engineering*
The University of Auckland, New Zealand
[2]*State Key Lab for Corrosion and Protection, Institute of Corrosion and Metal Protection,*
Academia Sinica, Shenyang, P R China

(Received April 17, 2000)

ABSTRACT

Micro-crystalline β-FeAl+Zr coatings on cast β-FeAl and 304S stainless steel substrates were produced with unbalanced magnetron sputter deposition technique. Isothermal oxidation in pure O_2 and a cyclic oxidation test in ambient air at 1000°C were carried out to assess the oxidation resistance of the coatings. The spallation resistance of the oxide scale formed on the coatings was superior compared with the uncoated alloys. After the oxidation in O_2, large voids at the cast FeAl/oxide interface were observed; while no obvious voids were found at the coating/oxide interface. Outward Al diffusion and S interfacial segregation were considered as the reasons for the formation of the voids. Recrystallization and grain growth of the coating was believed to play an important role in improving the spallation resistance. The chemical compatability of the coating with 304S stainless steel substrate was also discussed.

Key words: β-FeAl+Zr coating, unbalanced magnetron sputter deposition, oxidation

INTRODUCTION

Intermetallic alloys possess good high temperature properties, low specific densities and relatively low manufacturing cost. These unique properties have made them attractive as lightweight structural materials for high temperature applications. So far, some of them have been commercially used to make key components and protective coatings working at high temperatures in some industries, such as aircraft, automotive, and power generation /1/.

β-FeAl (Fe-37~49at.%Al) has low density, potentially lower cost than other intermetallics such as NiAl, and excellent high temperature corrosion resistance in oxidising and sulfidising environments /2,3/. When β-FeAl is used at high temperatures, alumina scale can be easily formed because of its relatively high Al content. However, heavy loss of the oxide scale always occurs during thermal cycling, which can cause severe degradation of the material /4/.

Another major disadvantage of β-FeAl is related to its mechanical strength at high temperatures. When it is used at temperatures above 600°C, it does not have sufficient strength for structural applications /3,5/, which prevents it from being an ideal candidate material for high temperature applications. Two possible solutions are suggested to overcome this problem, either to strengthen it by adding oxide dispersion such as Y_2O_3 and ZrO_2 /6,7/, or to use it as protective coatings on the substrates that have enough high temperature mechanical strength but poor high-temperature corrosion resistance /8/.

Even if overlay coatings of Fe-Al alloys have been produced by a few techniques, including thermal spray, electron-spark deposition, pack cementation, arc

welding /9/, and magnetron sputter deposition /10/, more work still needs to be done to assess their performance at high temperatures.

In the present work, β-FeAl+Zr coatings on β-FeAl and 304S stainless steel substrates were produced with unbalanced magnetron sputter deposition technique. Isothermal exposure in pure O_2 at 1000°C and a cyclic oxidation test in ambient air at 1000°C were carried out to evaluate the oxidation resistance of the coatings. The chemical compatibility of the coating with the 304S substrate at high temperature was also discussed.

EXPERIMENTAL PROCEDURE

The Fe-45at.%Al intermetallic alloy was produced by standard vacuum melting and casting using pure metals of Fe and Al (>99.9%) as raw materials. β-FeAl substrates and the sputter target were machined from the same cast plate. The dimensions of FeAl and 304S substrates were 2×10×15mm and 2×12×18mm respectively. The composition of 304S is Ni-8.0~10.0, Cr-18.0~20.0, Mn-2.0, Si-1.0, P-0.045, S-0.03 and Fe-Bal. (wt.%). Before deposition and oxidation, specimens were mechanically polished to 6 μm and ultrasonically cleaned with acetone.

Four 3mm-diameter Zr-plugs were tightly inserted in four 3mm-diameter holes along the erosion ring of the FeAl target to form a composite target of FeAl+Zr, whose design has been described in detail elsewhere /11/. Sputter deposition was carried out with an unbalanced magnetron-sputtering device using an Ar pressure of 5 mTorr. The distance between the substrate and the target was ~70mm, the substrate bias voltage was -50V, and the target current was 15-20 mA/cm^2. FeAl and 304S substrates were fixed in front of the target during deposition with only one side receiving deposition each time. Deposition time was 5 hours for each side. After depositions on both sides of the substrates, the total coating mass gain on each substrate was measured, from which the average coating thickness was estimated to be ~20 μm.

Isothermal oxidation testing in pure and dry O_2 atmosphere at 1000°C was carried out for 100 hours with a SANTRAM thermo-gravimatical analysis (TGA) station, during which mass change was recorded continuously. Cyclic oxidation testing in ambient air at 1000°C for 100 1-hr cycles was performed with a vertical furnace. The cycle time at temperature was 1 hr and the cooling time in air was 5 min. The process for the samples to move in and out of the furnace was automatically controlled by a timing system. Temperature accuracy in the hot zone of the furnace was controlled within ±5 K. The mass changes of the samples were measured after a number of cycles.

A scanning electron microscope (SEM) was used to observe the morphologies of the coatings and the oxide scales. X-ray diffraction (XRD) using a Philips PW 1729 X-ray source and a Philips 1050/25 goniometer attachment with Co-K_α radiation was conducted to identify the crystal structures of the coatings, the cast FeAl substrates, and the oxide products. A NanoScope® IIIa Atomic Force Microscopy (AFM) was used to observe the surface morphology of the coating. Composition of the coating was analysed by using Energy Dispersive Spectroscopy (EDS) in SEM.

RESULTS

1. Coating composition and structures

Composition of the β-FeAl+Zr coating was analysed to be Fe-45Al-0.5Zr (at.%) by EDS. Fig. 1 shows an AFM image of the coating surface and a SEM photograph of the fracture cross section. The coating microstructure is columnar and fine-grained with the average width of grain columns being less than 500 nm. XRD patterns for the coating and cast FeAl is shown in Fig.2. Both coating and cast FeAl show B2 (CsCl-type) phase structures.

2. Isothermal oxidation in pure O2

Fig.3 shows the kinetics of the coating and cast β-FeAl during isothermal oxidation testing in pure O_2 at 1000°C for 100 hours. The mass gains for the coating and the cast are in the same order of magnitude. The mass gain of the cast β-FeAl increased rapidly at the early stage of oxidation, slowed down after about 5 hours, and then oscillated in the range between 20 and

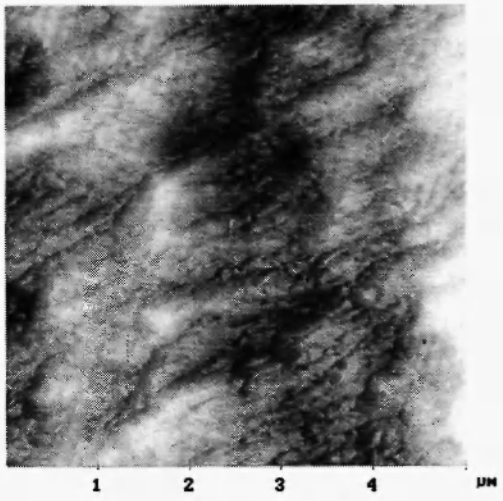

(a)

(b)

Fig. 1: (a) AFM image of coating surface and (b) SEM photograph of fracture coating cross section

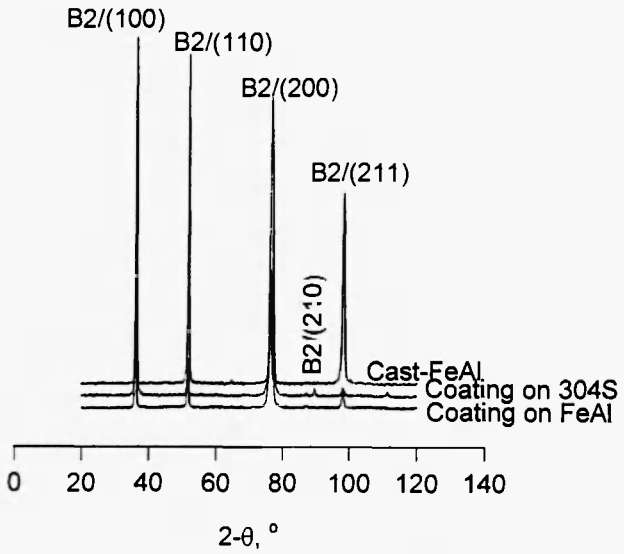

Fig. 2: XRD pattern of the β-FeAl+Zr coatings and the cast β-FeAl

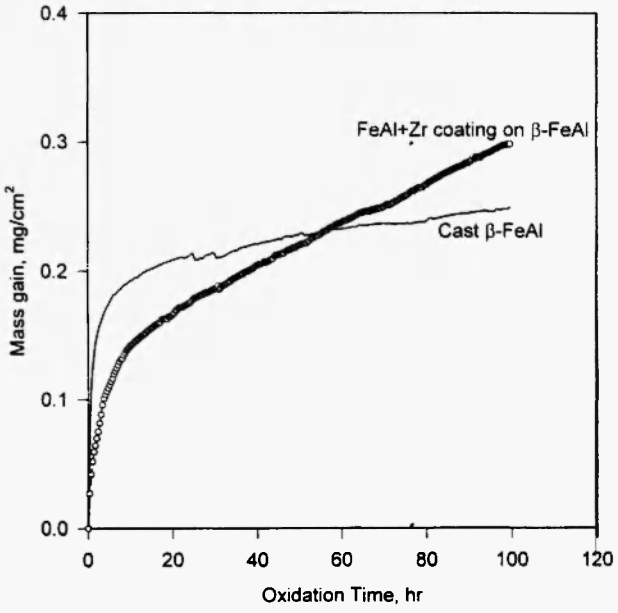

Fig. 3: The isothermal oxidation kinetics of the coating and the cast FeAl during the testing in pure oxygen at 1000°C for 100 hours

40 hours. The oscillation in the mass change recording might indicate spalling of the oxide scale. By contrast, the mass gain of the coating increased relatively smoothly during the oxidation, approximately following a parabolic rate law with a K_p value of 9.73×10^{-4} $mg^2/(cm^4h)$. Table 1 summarises the XRD results of the cast and coating after the isothermal oxidation, which indicate that α-Al_2O_3 was the main oxide product in both cases.

Fig.4 shows SEM photographs of the morphologies of the oxides formed on the cast β-FeAl and coating after isothermal oxidation in O_2 for 100 h. Ridge-like oxides formed on the cast β-FeAl and massive

Table 1

XRD results of the coating and cast FeAl after isothermal oxidation in O_2 at 1000°C for 100 h

Uncoated FeAl			FeAl-Zr coated		
d (Å)	I/I_{100}	Phase	d (Å)	I/I_{100}	Phase
3.504	4	A/012	3.493	5	A/012
2.895	23	B/100	2.889	3	B/100
2.563	7	A/104	2.564	10	A/104
2.102	4	A/113	2.094	5	A/110
2.048	100	B/110	2.048	100	B/110
1.672	7	B/111	1.672	27	B/111
1.611	3	A/116	1.613	6	A/116
1.449	8	B/200	1.183	88	B/211
1.183	9	B/211			

Note: A = α-Al_2O_3 phase, B = B2 phase

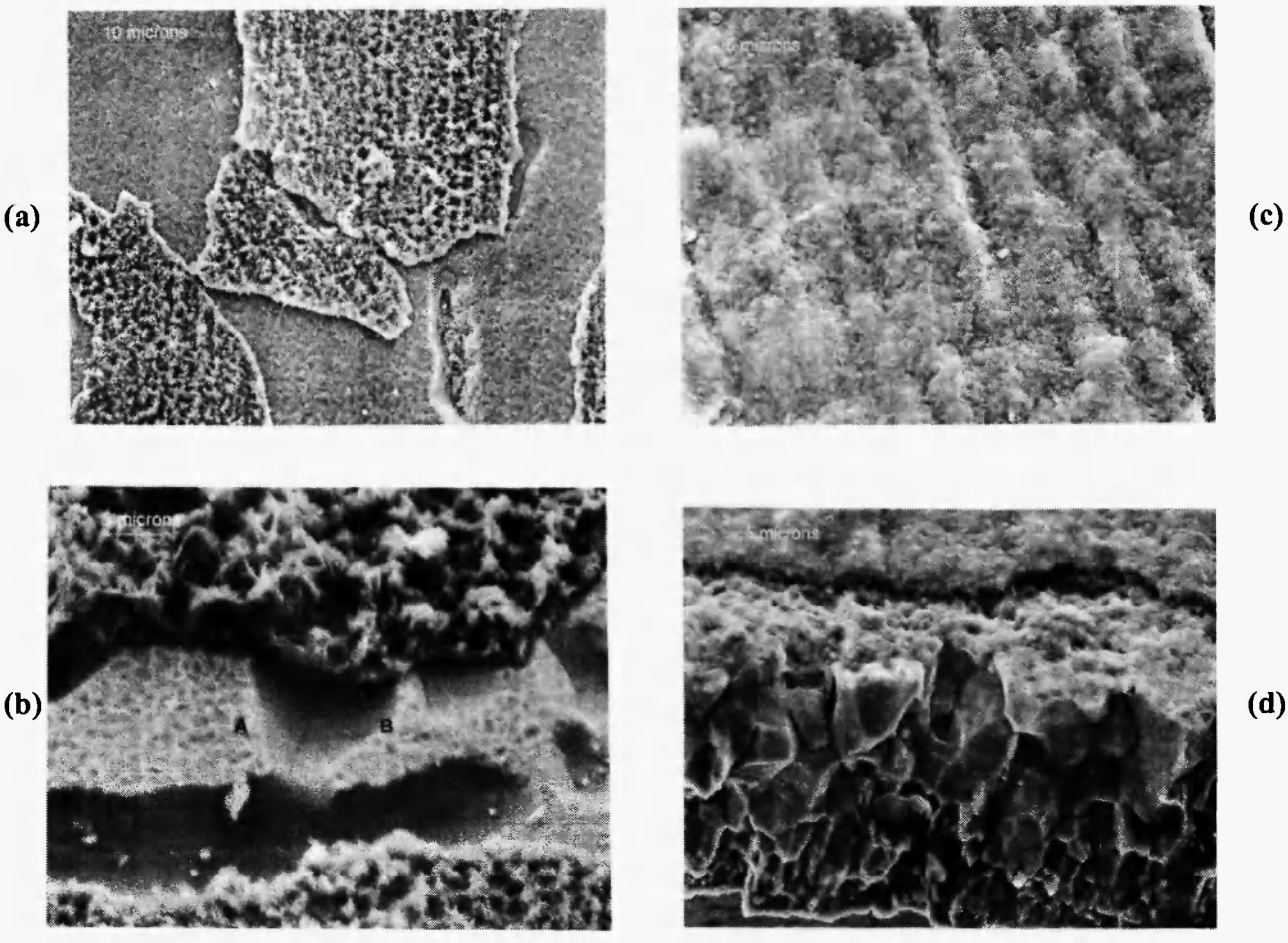

Fig. 4: SEM photographs of the morphologies of the oxides formed on the cast FeAl and coating after isothermal oxidation in O_2 for 100 h. (a) A plan-view of the oxide scale formed on the cast FeAl; (b) A 3-D view of the oxide scale on the cast FeAl; (c) A plan view of the oxide scale on the coating; and (d) A 3-D view of the fracture cross section of the coating after the oxidation; The samples were tilted by 45° in SEM. The oxidised coating was mechanically bent to obtain the fracture cross section.

spallation of oxide scale had occurred, Fig. 4(a). A 3-D view of the oxide cross-section, Fig. 4(b), showed that there were a small amount of whisker-type aluminas in the oxide. In a spalled region on the cast β-FeAl substrate, web-like grain imprints and concave voids with the average size of more than 5 μm were observed, as indicated by Arrows A and B respectively. It can be seen that the scale and the substrate were apparently detached at the voids. The oxide scales formed on the coatings, however, appeared to be fine-grained and intact without any spalled areas, Fig. 4(c). The fracture cross-section of the oxidised coating, Fig. 4(d), showed that the coating/oxide interface was relatively flat and compact with a thin fine-grained layer on top of the coarse coating grains. The scale remains in good contact to the coating.

3. Cyclic oxidation in air

Fig. 5 compares the cyclic oxidation kinetics of the coatings on β-FeAl and 304S substrates in a test in air at 1000°C for 100 1-hour cycles. The coating on FeAl substrate showed a smooth and low mass gain throughout the oxidation, while the coating on 304S exhibited a high mass gain with a breakaway after about 50 cycles. No mass losses could be observed from the oxidation kinetics. The uncoated alloys, however, showed severe mass losses as indicated by their cyclic oxidation kinetics measured under the same oxidation conditions.

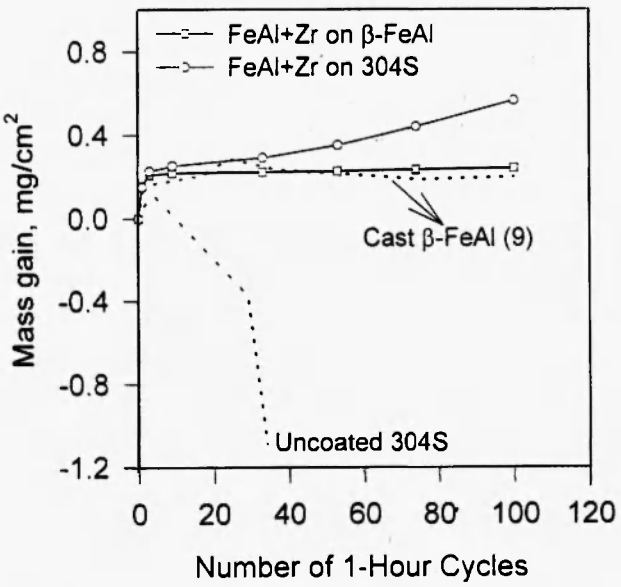

Fig. 5: Cyclic oxidation kinetics of the coatings on FeAl and 304S substrates during a test in air at 1000°C for 100 1-h cycles with the cycle time at temperature of 1 h. The dotted lines denote the cyclic oxidation kinetics of the uncoated alloys /9/.

Fig. 6 shows SEM photographs of the surface morphologies of the coatings on FeAl and 304S after the cyclic oxidation. Fine-grained oxides formed on both coatings. A SEM photograph of the metallographic cross-section of the coating on 304S after the cyclic

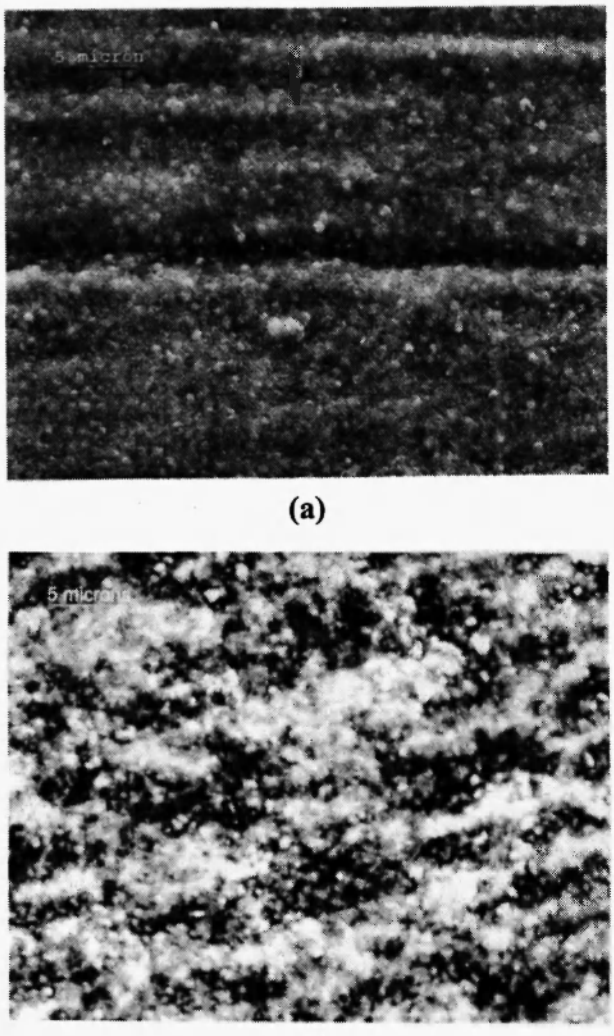

Fig. 6: SEM photographs of the surface morphologies of the coatings on FeAl and 304S after the cyclic oxidation in air for 100 1-h cycles; (a) the coating on FeAl, (b) the coating on 304S

oxidation and its EDS x-ray mapping are shown in Fig. 7. The mapping demonstrated that Al_2O_3 was formed as the external oxide layer and an inter-diffusion between the coating and the 304S substrate occurred with Al and Cr diffusing into the substrate and coating respectively.

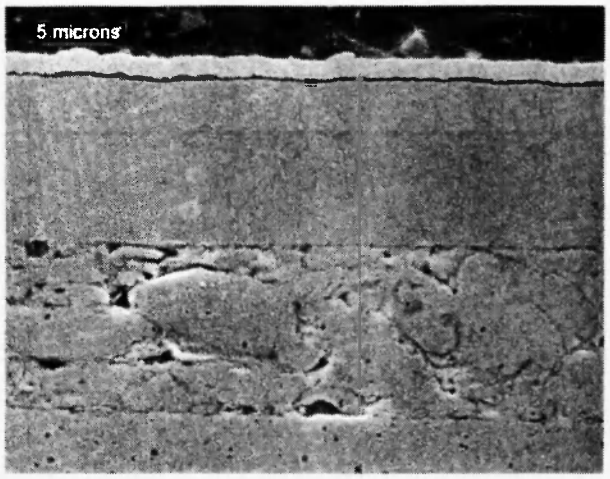

(a)

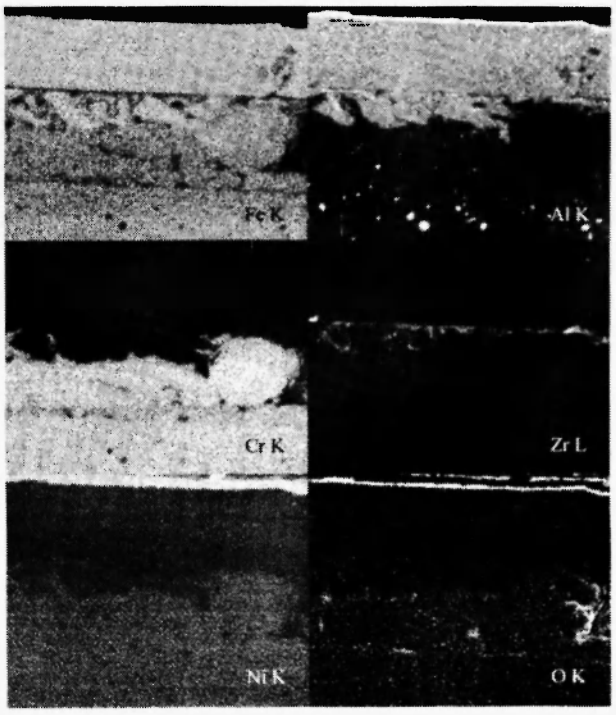

(b)

Fig. 7: (a) SEM photograph of the metallographic cross section of the coating on 304S after the cyclic oxidation in air for 100 1-h cycles and (b) its EDS x-ray mapping

DISCUSSION

Interfacial voids limit contact between the oxide scale and the substrate alloy and often act as precursors to spallation at the interface /12/. In the present work, large voids were observed in the exposed areas of the cast FeAl after the oxidation in O_2. The formation of the voids can be attributed to outward diffusion of Al ions during oxide scale growth /12,13/ and sulphur interfacial segregation /14,15/. The web-like imprints on the FeAl grains and the whisker-type oxides clearly showed that the transformation of metastable θ- to thermodynamically stable α-alumina had been occurring in the oxidation /16/. The growth of θ-alumina is predominantly controlled by outward Al diffusion following relatively fast oxidation kinetics. The rapid increase of mass gain at the early stage of oxidation for the cast β-FeAl, Fig. 3, was a good indication of the formation of θ-alumina. Therefore, the outward diffusion of Al ions to form θ-alumina might have been responsible for the generation of the vacancies at the alloy/oxide interface, which could then grow to large voids due to vacancy coalescence. The concave voids possessed smooth areas, showing a typical example of S segregation /17/, which could reduce the surface energy to accelerate the void formation and cause detachments between the scale and the substrate. In the present work, no attempts were made to desulphurize the cast β-FeAl alloy. It is believed that S contents in the cast alloy and the coating were at an average level that was sufficient for the interfacial segregation.

By contrast, no obvious voids at the coating/oxide interface can be observed. It has been clearly demonstrated that reactive elements such as Y and Zr can segregate at the alloy/oxide interface to seal the vacancies /12/, hold S in bulk and reduce its interfacial segregation /13/, and inhibit outward Al diffusion /18/. All of them may have played important roles in improving the oxide spallation resistance of the coating. Being predominantly controlled by oxygen inward diffusion along alumina grain boundaries, the alumina scale grows toward the oxide/alloy interface and results in a columnar microstructure. The thin fine-grained layer on the coating grains may represent the imprint of the alumina formed by inward oxygen diffusion.

Previous work /10/ demonstrated that undoped β-FeAl coating on the same material possessed better spallation resistance than the cast in a cyclic oxidation test in air at 1000°C. Ridge-like oxide containing θ-alumina was identified as main oxidation product formed on the coating. In this case, neither the elimination of outward Al diffusion nor lower S level could account for the improvement of oxide spalling resistance, but instead it was attributed to the effects related to the coating microstructure.

In the present work, the coating microstructural evolution during oxidation testing can be seen clearly. Before oxidation, the coating grains were columnar and microcrystalline (Fig. 1(b)), which were believed to be subjected to compressive stresses and in a high-energy state. After the oxidation exposure they became equiexed and much coarser (Fig. 4(d)), indicating that recrystallization and grain growth had occurred. This relaxation process resulted in plastic deformation on the oxide scale and the coating to release the stresses generated during scale growth and cooling and improved the scale adherence.

When β-FeAl is used as a coating material, the chemical compatibility of the coating with a different composition substrate must be considered /18/. In the present work, coating b showed inferior oxidation resistance compared with coating A. X-ray elemental mapping indicated that the inter-diffusion of Al and Zr had occurred at high temperature. At the coating/304S substrate interface, Zr and Al-rich compound was formed. This phase may be brittle and may have caused some detachment between the coating and substrate, where the substrate was exposed to the oxidising environment to result in the breakaway oxidation kinetics. The diffusion of Al to the substrate reduced the Al reservoir in the coating and shortened its service life. The diffusion of Cr into the coating, on the other hand, may have brought in benefits to the coating because Cr is believed to have positive effects on high temperature corrosion behaviour of FeAl intermetallics /3,8/. More work needs to be done to evaluate the compatibility of β-FeAl coating with the different alloys before using it as a coating material.

CONCLUSION

Microcrystalline β-FeAl+Zr coatings on the cast FeAl and 304S stainless steel substrates showed superior scale spallation resistance compared with the uncoated alloys. After the oxidation in O_2, concave voids at the cast FeAl/oxide interface were observed, which may have caused severe scale spallation. The outward Al diffusion and S interfacial segregation were considered to be the reasons for the formation of the voids. No obvious voids, however, could be found on the coating. Recrystallization and grain growth of the coating microstructure occurring during oxidation played an important role in improving the spallation resistance. Inter-diffusion between the coating and 304S substrate took place during the oxidation at 1000°C. A brittle phase rich in Zr and Al was observed at the coating/304S interface, which resulted in the detachment of the coating from the substrate and deteriorated the coating protective ability.

ACKNOWLEDGEMENTS

This work was supported by a New Zealand FoRST Post-Doctoral Fellowship under the contract of UoA815. The authors would like to thank Drs J. Chen, G. Wright, W G. Ferguson, and M. Hyland for various supports.

REFERENCE

1. V.K. Sikka, In: *Oxidation and Corrosion of Intermetallic Alloys*, ed by G. Welsch and P.D. Desai, 1996, 1.
2. G. Sauthoff, In: *Oxidation of Intermetallics*, ed by H.J. Grabke and M. Schutze, Wiley-Vch, 1996, 3.
3. R. Prescott and M.J. Graham, *Oxidation of Metals*, **38**, 73 (1992).
4. J.L. Smialek, J. Doychak and D.J. Gaydosh, *Oxidation of Metals*, 34, 257 (1990).

5. P.F. Tortorelli, J.H. DeVan, G.M. Goodwin and M. Howell, In: *Elevated Temperature Coatings: Science and Technology I*, ed by N.B. Dahotre, J.M Hampikian and J.J. Stiglich, TMS, Warrendale, Pennsylvania, 1995, 203.
6. B.A. Pint, J. Leibowitz, and J.H. DeVan, *Oxidation of Metals*, **51**, 181 (1999).
7. B.A. Pint, P.F. Tortorelli and I.G. Wright, In: *Oxidation of Intermetallics*, eds. by H. J. Grabke and M. Schutze, Wiley-Vch, New York, 1996, 183.
8. P.F. Tortorelli and J.H. DeVan, *Materials Science and Engineering*, **A153**, 573 (1992).
9. P.F. Tortorelli and K. Natesan, *Materials Science and Engineering*, **A258**,115 (1998).
10. Z. Liu, W. Gao and F. Wang, *Scripta Materialia*, **39**, 1497 (1998).
11. Z. Liu, W. Gao and M. Li, *Oxidation of Metals*, **51**, 403 (1999).
12. B.A. Pint, *Oxidation of Metals*, **48**, 303 (1997).
13. B.A. Pint, A.J. Garratt-Reed and L.W. Hobbs, *Materials at High Temperatures*, **13**, 3 (1995).
14. H.J. Grabke, D. Wiemer and H. Viefhaus, *Applied Surface Science*, **47**, 243 (1991).
15. J.K. Tien and F.S. Pettit, *Metallurgical Transactions*, **3**, 1587 (1972).
16. G.C. Rybicki and J.L. Smialek, *Oxidation of Metals*, **31**, 275 (1989).
17. D.R. Sigler, *Oxidation of Metals*, **29**, 23 (1988).
18. B.A. Pint, *Oxidation of Metals*, **45**, 1 (1996).
19. L. Singheiser, H.W. Grunling and K. Schneider, *Surface and Coatings Technology*, **42**, 101 (1990).